

**Co-delivery of 2-DG and V9302 via a Prodrug Micellar Formulation for Synergistic Targeting of Metabolism in Cancer**

by

**Zhangyi Luo**

BS, Sun Yat-sen University, 2017

Submitted to the Graduate Faculty of

School of Pharmacy

of the requirements for the degree of

Master of Science

University of Pittsburgh

2019

UNIVERSITY OF PITTSBURGH  
SCHOOL OF PHARMACY

This thesis/dissertation was presented

by

**Zhangyi Luo**

It was defended on

March 25, 2019

and approved by

Song Li, Professor, Department of Pharmaceutical Science

Xiaochao Ma, Associate Professor, Department of Pharmaceutical Science

Da Yang, Assistant Professor, Department of Pharmaceutical Science

Thesis Advisor/Dissertation Director: Song Li, Professor, Department of Pharmaceutical Science

Copyright © by Zhangyi Luo

2019

## **Co-delivery of 2-DG and V9302 via a Prodrug Micellar Formulation for Synergistic Targeting of Metabolism in Cancer**

Zhangyi Luo, BS

University of Pittsburgh, 2019

The unique metabolic demand of cancer cells suggests a new therapeutic strategy targeting the metabolism in cancers. V9302 is a recently reported inhibitor of ASCT2 amino acid transporter which shows promising antitumor activity by blocking glutamine uptake. However, its poor solubility in aqueous solutions and tumor cells' compensatory metabolic shift to glucose metabolism may limit the antitumor efficacy of V9302. 2-Deoxyglucose (2-DG), a derivative of glucose, has been developed as a potential antitumor agent through inhibiting glycolysis in tumor cells. In order to achieve enhanced antitumor effect by inhibiting both metabolic pathways, a 2-DG prodrug-based micellar carrier (POEG-p-2DG) was developed. POEG-p-2DG well retained the pharmacological activity of 2-DG in vitro and in vivo. More importantly, POEG-p-2DG could self-assemble to form micelles that were capable of loading V9302 to achieve co-delivery of 2-DG and V9302. V9302-loaded POEG-p-2DG micelles were small in sizes (~10nm), showed a slow kinetics of drug release and demonstrated targeted delivery to tumor. In addition, V9302 loaded POEG-p-2DG micelles exhibited improved anti-tumor efficacy both in vitro and in vivo with decreased toxicity compared to free drug combination. These results suggest that POEG-p-2DG prodrug micelles may serve as a dual functional carrier for V9302 to achieve synergistic targeting of metabolism in cancers.

## Table of Contents

<b>Table of Contents .....</b>	<b>v</b>
<b>1.0 Introduction.....</b>	<b>1</b>
<b>1.1 Targeting cancer metabolism is a potential strategy for cancer treatment .....</b>	<b>1</b>
<b>1.2 Effect and limitation of 2-DG as a glycolysis inhibitor for cancer treatment .....</b>	<b>1</b>
<b>1.3 V9302 as a glutamine metabolism inhibitor for cancer treatment .....</b>	<b>2</b>
<b>1.4 POEG-p-2DG is an ideal carrier to co-deliver 2DG and V9302 for synergistically targeting the cancer metabolism .....</b>	<b>3</b>
<b>1.5 Overview of thesis.....</b>	<b>4</b>
<b>2.0 Experimental Section.....</b>	<b>5</b>
<b>2.1 Material .....</b>	<b>5</b>
<b>2.2 Methods .....</b>	<b>6</b>
<b>2.2.1 Synthesis of VBSS monomer .....</b>	<b>6</b>
<b>2.2.2 Synthesis of POEG-p-2DG polymer .....</b>	<b>6</b>
<b>2.2.3 Characterization of the synthesized monomer and polymers.....</b>	<b>7</b>
<b>2.2.4 Preparation and Characterization of Blank or V9302-loaded POEG-p-2DG micelles</b>	<b>7</b>
<b>2.2.5 In Vitro Cytotoxicity Assay .....</b>	<b>8</b>
<b>2.2.6 Real-time PCR.....</b>	<b>9</b>
<b>2.2.7 Analysis of Glucose and Glutamine Metabolism .....</b>	<b>10</b>
<b>2.2.8 Western Blot .....</b>	<b>11</b>
<b>2.2.9 In vivo Biodistribution with Near-Infrared Fluorescence Imaging .....</b>	<b>11</b>

2.2.10 In Vivo Therapeutic Study .....	12
2.2.11 Histochemical Staining .....	12
2.2.12 ALT/AST and Creatinine Assessment .....	13
<b>3.0 Result.....</b>	<b>14</b>
3.1 Synergistic effect of V9302 and 2-DG on cancer cell growth .....	14
3.2 Synthesis and Characterization of the POEG-p-2DG micelles .....	16
3.3 <i>In vitro</i> Drug Release Study .....	19
3.4 <i>In vitro</i> Cytotoxicity of V9302 loaded POEG-p-2DG Micelles .....	20
3.5 Effect of V9302-loaded POEG-p-2DG micelle on glucose and glutamine metabolism	
21	
3.6 Biodistribution study.....	23
3.7 <i>In vivo</i> Therapeutic and Toxicological Study .....	26
<b>4.0 Discussion.....</b>	<b>29</b>
<b>Appendix A Supplementary Materials .....</b>	<b>33</b>
A.1 <sup>1</sup> H-NMR .....	33
A.2 H&E staining of liver .....	35
<b>Bibliography .....</b>	<b>36</b>



## List of Tables

Table. 1 Synergistic Antiproliferative Activity of V9302 and 2-DG in Cancer Cells.....	15
--	----



## List of Figures

Figure. 1 Overview of POEG-p-2DG carrier and its function.....	4
Figure. 2 Synergistic effect between V9302 and 2-DG in inhibiting the proliferation of different tumor cell lines.....	15
Figure. 3 Synthesis Scheme of POEG-p-2DG Conjugate .....	17
Figure. 4 DLS and TEM Characterization of (A)POEG-p-VBSS, (B)POEG-p-2DG and (C)V9302-loaded POEG-p-2DG micelles.....	18
Figure. 5 Measurement of Critical Micelle Concentration of POEG-p-2DG micelles.....	18
Figure. 6 Cumulative V9302 release profile from POEG-p-2DG micelles and free V9302 in 48h. ....	19
Figure. 7 Cytotoxicity of POEG-p-2DG and V9302-loaded POEG-p-2DG micelles .....	21
Figure. 8 V9302/POEG-p-2DG have inhibition effect on both glucose metabolism and glutamine metabolism.....	23
Figure. 9 In vivo(A) and ex vivo(B-D) of NIRF imaging of biodistribution of POEG-p-2DG formulation.....	25
Figure. 10 Enhanced in vivo antitumor activity of V9302-loaded POEG-p-2DG micelle.....	27
Figure. 11 Histological analysis of tumor tissues by ki67 staining .....	27
Figure. 12 Toxicological assay of V9302-loaded POEG-p-2DG micelle .....	28

## List of Supplementary Figure

Figure S 1 $^1\text{H-NMR}$ of VBSS monomer.....	33
Figure S 2 $^1\text{H-NMR}$ of POEG-p-VBSS polymer backbone .....	34
Figure S 3 $^1\text{H-NMR}$ of POEG-p-2DG .....	35
Figure S 4 H&E staining of liver .....	35



## **1.0 Introduction**

### **1.1 Targeting cancer metabolism is a potential strategy for cancer treatment**

Cancer cells exhibit a pronounced metabolic reprogramming to support their abnormal proliferation.[1-3] For example, additional nutrients are consumed by cancer cell. These nutrients are diverted into macromolecular synthesis pathway. The rewired metabolic pathways help cancer cell balance the biosynthetic processes with sufficient ATP production. These alterations of metabolic pathways represent attractive therapeutic targets.[4, 5].

### **1.2 Effect and limitation of 2-DG as a glycolysis inhibitor for cancer treatment**

One of the most well-studied metabolic alteration in cancer cell is the increase and the dependency on anaerobic glycolysis pathway for ATP generation despite availability of sufficient oxygen to oxidize glucose completely. This is known as the “Warburg Effect”, which is regarded as a metabolic hallmark of aggressive tumors[6, 7]. Accordingly, targeting abnormal glycolysis for the treatment of cancer has been explored previously as a therapeutic approach[8]. Of all the glycolysis inhibitors that were evaluated, 2-deoxyglucose (2-DG) is the one that has been best characterized in animal model studies[9-11] and human clinical trials[12-14], 2-DG is a glucose analog and is converted by hexokinase to phosphorylated 2-DG, which is trapped inside the cell. The phosphorylated 2-DG can further inhibit the production of glucose-6-phosphate from glucose. As a direct consequence of 2-DG treatment, intracellular ATP is depleted, which ultimately

suppresses cell proliferation in vitro. However, normal cell also requires glycolysis to produce energy. The rapid clearance of 2-DG and its discriminative nature in tissue distribution has hindered its further clinical application. Serious side effects were observed in 2-DG clinical trial, such as hypoglycemia, QTc prolongation and cardiac arrest. Most importantly, preclinical and clinical studies indicate that 2-DG treatment, when provided as a single agent, provides limited therapeutic benefits.[15, 16] Therefore, development of combination therapy as well as a strategy for targeted delivery of 2-DG is necessary.

### **1.3 V9302 as a glutamine metabolism inhibitor for cancer treatment**

Apart from glucose, emerging researches demonstrate a critical role for glutamine in energy generation, biosynthesis and cell homeostasis of cancer cells[17]. Glutamine is transported into cell largely through solute carrier family 1 neutral amino acid transporter member 5 (SLC1A5; also known as ASCT2)[18]. After being transported into cell, glutamine itself can contribute to nucleotide biosynthesis. It can also be involved in protein trafficking and folding through its contribution to the synthesis of uridine diphosphate N-acetylglucosamine. Alternatively, it can be converted to glutamate by mitochondria glutaminase (GLS). Glutamate can contribute to the synthesis of glutathione which is critical for the maintenance of cell homeostasis, or more importantly, be converted to  $\alpha$ -ketoglutarate ( $\alpha$ KG) by glutamate dehydrogenase or aminotransferase.  $\alpha$ KG is the central metabolite of glutamine metabolism that can enter the TCA cycle, through which glutamine pathway and glucose pathway are bridged and highly incorporated with each other[19-21]. Because of Warburg effect, most glucose-derived carbons are secreted as lactate instead of entering TCA cycle as pyruvate. This leads to glutamine anaplerosis that utilizes

$\alpha$ KG to compensate the carbon source in TCA cycle and refill the TCA functions to guarantee the survival and proliferation of cancer cells. The alteration of glutamine demanding is also known as “glutamine addicted”—i.e., cancer cell is highly glutamine-consuming for maintaining the survival or proliferation compared to normal cell[3, 22]. Based on this feature, several compounds have been developed to target the abnormal dependency on glutamine of cancer cell[23, 24]. For example, CB-839 is a GLS inhibitor that is under phase II clinical trial[25, 26]. Also, V9302, a recently reported inhibitor of glutamine transporter ASCT2, showed promising antitumor response by inhibiting glutamine uptake in preclinical studies[18, 27]. However, similar to the glutamine anaplerosis upon inhibition of glycolysis, interference of glutamic metabolism leads to upregulation of glucose metabolism.[27-29]. Although the mechanism is not clearly understood, the compensatory shift between glucose and glutamine metabolism suggests the importance of developing a combination strategy to target both metabolic pathways. It is also important to develop a strategy to achieve selective delivery of the metabolism inhibitors to tumor to improve the efficacy, and more importantly, decrease the systemic toxicity.

#### **1.4 POEG-p-2DG is an ideal carrier to co-deliver 2DG and V9302 for synergistically targeting the cancer metabolism**

Here, we reported a 2-DG-based prodrug polymeric carrier (POEG-p-2DG) to achieve synergistic targeting of cancer metabolism. POEG-p-2DG polymer can serve as a depot system allowing the release of active 2-DG over a prolonged period of time. Moreover, POEG-p-2DG polymer can self-assemble to form micelles for codelivery of V9302. We hypothesize that selective codelivery of V9302 and 2-DG via POEG-p-2DG-based nanocarrier can not only



## 2.0 Experimental Section

### 2.1 Material

V9302 was synthesized and purified following a published paper[30]. 4-Vinylbenzyl chloride, 4,4-dithiodibutyric acid, triethylamine, 4-Cyano-4-(phenyl-carbonothioylthio)pentanoic acid, poly(Ethylene glycol)methyl ether methacrylate (average Mn = 950), 2,2-Azobis(isobutyronitrile)(AIBN), Dulbecco's Modified Eagle's Medium (DMEM), RPMI 1640 Medium, trypsin-EDTA solution, 3-(4,5-dimethylthiazol-2-yl)-2,5-diphenyl tetrazolium bromide (MTT) were purchased from Sigma-Aldrich (MO, U.S.A). 2-deoxy-D-glucose was purchased from AK Scientific Inc. (CA, U.S.A.). Antibody against ASCT2 was purchased from Cell Signaling Technology, Inc. (MA, U.S.A). SuperSignal™ West Fento Maximum Sensitivity Substrate Kit and Pierce™ RIPA buffer were purchased from Thermo Scientific (MA, U.S.A). Fetal bovine serum (FBS), penicillin-streptomycin solution and Trizol lysis reagent were purchased from Invitrogen (NY, U.S.A.). QuantiTect Reverse Transcription Kit was purchased from Qiagen (MD, U.S.A). EnzyChrom Glutamine Assay kit was purchased from BioAssay Systems (CA, USA), Glucose Colorimetric/Fluorometric Assay Kit and Lactate Colorimetric/Fluorometric Assay Kit were purchased from BioVision Inc. (CA, USA). ALT/SGPT Liqui-UV Test Kit and AST/SGOT Liqui-UV Test Kit were purchased from Stanbio Laboratory (TX, USA).

## 2.2 Methods

### 2.2.1 Synthesis of VBSS monomer

Vinylbenzyl chloride (305.2mg, 2mM), 4,4'-Dithiodibutyric acid (2.38g, 10mM) and  $K_2CO_3$  (1.38g 10mM) were mixed in 10mL DMF and reacted at 50 °C under stirring. After 16h, the mixture was cooled down to room temperature and 90mL methylene dichloride is added to extract the product. The mixture was centrifuged at 4500 rpm for 10min. The precipitate was washed with methylene dichloride for 2 times and all the supernatant was collected, washed with brine for three times, and then dried with anhydrous sodium sulfate. The VBSS monomer was purified by column chromatography with ethyl acetate/petroleum ether (v/v=1/3 to 1/1) as the elution buffer.

### 2.2.2 Synthesis of POEG-p-2DG polymer

4-Cyano-4-(thiobenzoylthio)pentanoic acid (15.2mg, 0.0545 mmol), AIBN (7.2mg, 0.0446 mmol), VBSS monomer (880mg, 2.79 mmol), OEG950 monomer (880mg, 0.924 mmol) and dried tetrahydrofuran (3.2mL) were added into a Schlenk tube. The Schlenk tube was placed in oil bath and stirred at 80°C with  $N_2$  protection overnight after deoxygenation with three freeze-thawing cycles.

### **2.2.3 Characterization of the synthesized monomer and polymers**

<sup>1</sup>H NMR spectrum was examined on a Varian-400 FT-NMR spectrometer at 400.0 MHz with CDCl<sub>3</sub> as the solvent. Molecular weight (M<sub>n</sub> and M<sub>w</sub>) and distribution (M<sub>w</sub>/M<sub>n</sub>) of the synthesized polymers were measured by gel permeation chromatography (GPC) performed on a Waters 515 HPLC pump and a Waters 717 Plus Autosampler equipped with a Waters 2414 refractive index detector. Tetrahydrofuran (THF) was used as the eluent with a flowing rate of 1.0 mL/min at 35 °C. A series of commercial polystyrene standards with narrow molecular weight distribution were applied to calibrate the GPC elution traces.

### **2.2.4 Preparation and Characterization of Blank or V9302-loaded POEG-p-2DG micelles**

V9302 solution (10mg/mL in methylene chloride) was mixed with POEG-p-2DG polymers (20 mg/mL in methylene chloride) at different carrier/drug weight ratios. The solvent was removed by nitrogen flow to produce a thin film of carrier/drug mixture, which was further dried in vacuum for 2 h to remove any remaining solvent. Then the thin film was hydrated and gently vortexed in PBS to form V9302-loaded POEG-p-2DG micelles.

The average diameter and the size distribution of POEG-p-2DG micelles were assessed via a Zetasizer (DLS). The morphology of POEG-p-VBSS polymer backbone, POEG-p-2DG blank micelles and drug-loaded micelles was observed by transmission electron microscopy (TEM).

The CMC of POEG-p-2DG micelles was determined by using Nile red as a fluorescence probe as described previously [29].

The kinetics of V9302 in vitro release from V9302/POEG-p-2DG was studied using a dialysis method. Briefly, 1mL of V9302/ POEG-p-2DG micelles containing 6mg of V9302 were placed in a clamped dialysis bag (MWCO 3.5kDa) and immersed in 25mL of 0.1M PBS buffer solution containing 0.5% (w/v) Tween 80 with or without 10mM GSH. The experiment was performed in an incubation shaker at 37 °C at 100 rpm. At selected time intervals, both 10 $\mu$ L V9302/POEG-p-2DG micelle solution in the dialysis bag and 1mL medium outside the dialysis bag were withdrawn while same amount of fresh medium was added to replenish. For comparison, free V9302 dissolved in 2% DMSO was included as free diffusion control. The V9302 release from micelles was measured by Waters e2695 HPLC system equipped with a Waters 2489 UV detector. Phosphoric acid (0.1%)/Methanol (v/v=45/55) was used as eluent with the flow rate of 1mL/min at 30 °C. V9302 was detected by UV at 276/227nm wave length.

### **2.2.5 In Vitro Cytotoxicity Assay**

Cytotoxicity assay was performed on 4T1.2 mouse breast cancer cell line, CT26 mouse colon cancer cell line, 3LL mouse lung cancer cell line, PANC-2 mouse pancreatic cancer cell line, MCF-7 human breast cancer cell line, MDA-MB-231 human breast cancer cell line, HCT116 human colon cancer cell line and A549 human lung cancer cell line. Cells were seeded in 96-well plates at various densities respectively (1x10<sup>3</sup> cells per well for 4T1.2, CT26, 3LL, PANC-2, HCT116, A549 and 5x10<sup>3</sup> cells per well for MCF-7, MDA-MB-231) followed by 24 h of incubation in DMEM or RPMI 1640 with 10% FBS and 1% streptomycin/penicillin.

To evaluate the combinational effect of 2-DG and V9302, cells were treated with various concentrations of free 2-DG, free V9302, and the combination of both respectively for 48 h. To examine the cytotoxicity of drug-loaded POEG-p-2DG micelles, free V9302, blank POEG-p-2DG and V9302/POEG-p-2DG (w/w ratio POEG-p-2DG:V9302=20:1) were incubated with cells for 48h before MTT assay was performed.

MTT assay and the calculation of cell viability were performed as described before. The anti-proliferation data for single drug and combination treatment were fitted to an inhibitory, normalized dose-response model with variable slope ( $Y = 100 / (1 + 10^{((\text{LogEC50}-X) * \text{HillSlope}))}$ ); (GraphPad Prism, San Diego, CA)

#### **2.2.6 Real-time PCR**

Real-time PCR studies were performed on 4T1.2 mouse breast cancer cell line, CT26 mouse colon cancer cell line, MDA-MB-231 human breast cancer cells and HCT116 human colon cancer cell line. 4T1.2, CT26 and HCT116 ( $2 \times 10^4$  cells/well) or MDA-MB-231 ( $6 \times 10^4$  cells/well) cells were seeded in 6-well plates followed by 24 h of incubation in DMEM (4T1.2, MDA-MB-231) or RPMI 1640 (CT26, HCT116) containing 10% FBS and 1% streptomycin/penicillin. After 24 hours, medium was replaced with medium with 2% FBS containing free V9302, blank POEG-p-2DG, V9302/POEG-p-2DG, free 2-DG (0.5 mM) that equal to 2-DG amount in POEG-p-2DG as well as free 2-DG of much higher concentration (10mM). After 48 hours, total cellular RNA was extracted using the TRIzol lysis reagent. cDNA was generated from the purified RNA using QuantiTect Reverse Transcription Kit according to the manufacturer's instructions. The cDNAs corresponding to different enzymes examined were amplified by PCR using the specific primers respectively. (supplementary form) Quantitative real-time PCR was performed using SYBR Green

Mix on a 7900HT Fast Real-time PCR System. Relative target mRNA levels were analyzed using delta-delta-Ct calculations and normalized to GAPDH.

### **2.2.7 Analysis of Glucose and Glutamine Metabolism**

The glutamine metabolism is determined by measuring the glutamine concentration intracellularly. The cells were first cultured under glutamine-deprived medium for 6 h to remove all the endogenous glutamine. Then different drug treatments were applied, along with normal RPMI medium. After 24 h, cells were trypsinized, gently washed three times with ice-cold PBS, and then resuspended in cold PBS. Afterwards, the cell suspension was sonicated on ice for 60 s with an amplitude of 50%, and the resulting cell debris was removed by centrifugation at 14,000 rpm for 10 min at 4 °C. The cell supernatant was transferred to a new microtube for immediate measurements. Glutamine measurement was determined using the EnzyChrom Glutamine Assay kit according to manufacturer's protocol. Total protein amount of cell extracts was measured using BCA protein assay. Intracellular glutamine levels were expressed as glutamine concentration normalized to protein concentration and control. The experiment was performed in triplicate.

The glucose metabolism is determined by measuring the glucose and lactate concentration in the cell culture medium. Cells for each experimental group were cultured in RPMI 1640 for 48 h with different treatments. Then cell culture medium of each group was collected and determined by using Glucose Colorimetric/Fluorometric Assay Kit and Lactate Colorimetric/Fluorometric Assay Kit according to manufacturer's protocol. Total protein amount of cell extracts was measured using BCA protein assay. Glucose uptake and lactate production were calculated by

comparing with the glucose or lactate amount in fresh medium and then normalized to protein concentration and control. The experiment was performed in triplicates.

### **2.2.8 Western Blot**

Western blotting was performed to evaluate the ASCT2 glycosylation in MDA-MB-231 and HCT116 cells. Cells grown in six-wells plates with 80% confluency were treated with free V9302, blank POEG-p-2DG micelles, V9302/POEG-p-2DG, and 10mM 2-DG respectively for 24 h. Cells were washed twice with pre-cooled PBS and lysed in Pierce™ RIPA buffer for 40 min in 4°C. Protein concentrations were determined by BCA method, and equal amounts of total protein lysate were resolved on a 10% SDS-PAGE and subsequently transferred to a nitrocellulose membrane. Membranes were blocked with 5% nonfat milk in PBS for 1 h prior to incubation with rabbit anti-ASCT2 primary antibody dissolved in PBST (DPBS with 0.1% Tween 20) overnight at 4°C. The blots were washed with PBST and then probed with goat antirabbit IgG for 1 h at room temperature followed by chemiluminescence detection by SuperSignal™ West Fento Maximum Sensitivity Substrate.  $\beta$ -Actin or GAPDH was used as a loading control.

### **2.2.9 In vivo Biodistribution with Near-Infrared Fluorescence Imaging**

DiR-loaded POEG-p-2DG micelles were prepared similarly to V9302-loaded POEG-p-2DG micelles at a POEG-p-2DG to DiR ratio of 20/1 (w/w). DiR-loaded POEG-p-2DG micelles were injected to 4T1 tumor bearing mice at a DiR dose of 1 mg/kg. At 4 hours and 24 hours, the mice were imaged by IVIS 200 system (Perkin Elmer, USA) at a 60s exposure time with excitation

at 730 nm and emission at 835nm. The mice were then sacrificed and perfused. Then major organs were dissected and subjected to ex vivo imaging.

#### **2.2.10 In Vivo Therapeutic Study**

The in vivo antitumor efficacy of the V9302-loaded POEG-p-2DG micelles was tested in a syngeneic 4T1.2 mouse breast cancer model. 4T1.2 cells ( $2 \times 10^5$  in 20  $\mu$ L PBS) were inoculated s.c. at the right mammary fat pad of female BALB/c mice. When the tumor volume reached  $\sim 50$  mm<sup>3</sup>, mice were randomly divided into 6 groups (n=5), and treated via tail vein injection with DPBS, blank POEG-p-2DG micelles, V9302-loaded POEG-p-2DG micelles and V9302/2-DG free drug combination through i.p or i.v injection respectively, at a V9302 dose of 60mg/kg. The treatments were first conducted every two days for 2 times and then every 3 days for the rest 3 times. Tumor sizes were measured with the digital caliper every three days following the initiation of the treatment and calculated by the formula:  $(L \times W^2)/2$ , where L is the longest and W is the shortest in tumor diameters (mm). Body weights were also monitored for the indication of toxicity. On day 23 post injection, all mice were sacrificed and tumor tissues were collected for weight, photography and H&E staining.

#### **2.2.11 Histochemical Staining**

After completion of the in vivo therapy study, tumor tissues and liver tissue were excised and fixed in PBS solution containing 10% formaldehyde, followed by embedment in paraffin. The paraffin-embedded tumor samples were sectioned into slices at 5  $\mu$ m using an HM 325 Rotary Microtome. The slices were then stained with hematoxylin and eosin (H & E) for histopathological

examination or ki67 immunostaining for cell proliferation by using Zeiss Axiostar plus Microscope (PA, USA).

### **2.2.12 ALT/AST and Creatinine Assessment**

Mouse blood was collected after sacrifice and centrifuged (12500 rpm, 4°C), and serum was collected for blood biochemical assessment. ALT/AST were measured by ALT/SGPT liqui-UV assay kit or AST/SGPT liqui-UV assay kit following manufacturer's protocol. Creatinine was measured by QuantiChrom™ Creatinine Assay Kit according to manufacturer's protocol.

### 3.0 Result

#### 3.1 Synergistic effect of V9302 and 2-DG on cancer cell growth

In order to assess the synergistic effect between V9302 and 2-DG, the proliferation inhibitory activity of V9302 and 2-DG, alone or in combination, was examined on breast cancer cell lines and colon cancer cell lines. As shown in Fig. 2, V9302 or 2-DG alone showed a concentration-dependent inhibition of proliferation in 4T1 breast cancer cell line(A). It is also apparent that the combination of the two drugs could result in a significant improvement in the level of inhibition of cell growth. Similar synergistic effects between 2-DG and V9302 were also found in MCF-7(B), MDA-MB-231(C), CT26(D) and HCT116(E). Combination Index was then calculated to further assess the potential synergistic effect between V9302 and 2-DG through the equation  $CI = (d1/IC_{501}) + (d2/IC_{502})$ , with  $IC_{501}$  or  $IC_{502}$  being the  $IC_{50}$  of V9302 or 2-DG monotherapy respectively, while  $d1$  being the concentration of V9302 required to achieve 50% killing effect of combination treatment at  $d2(2-DG) = 0.6mM$ . The CI values of all tested cell lines were calculated to be less than one, an indication of the synergistic effect between 2-DG and V9302.

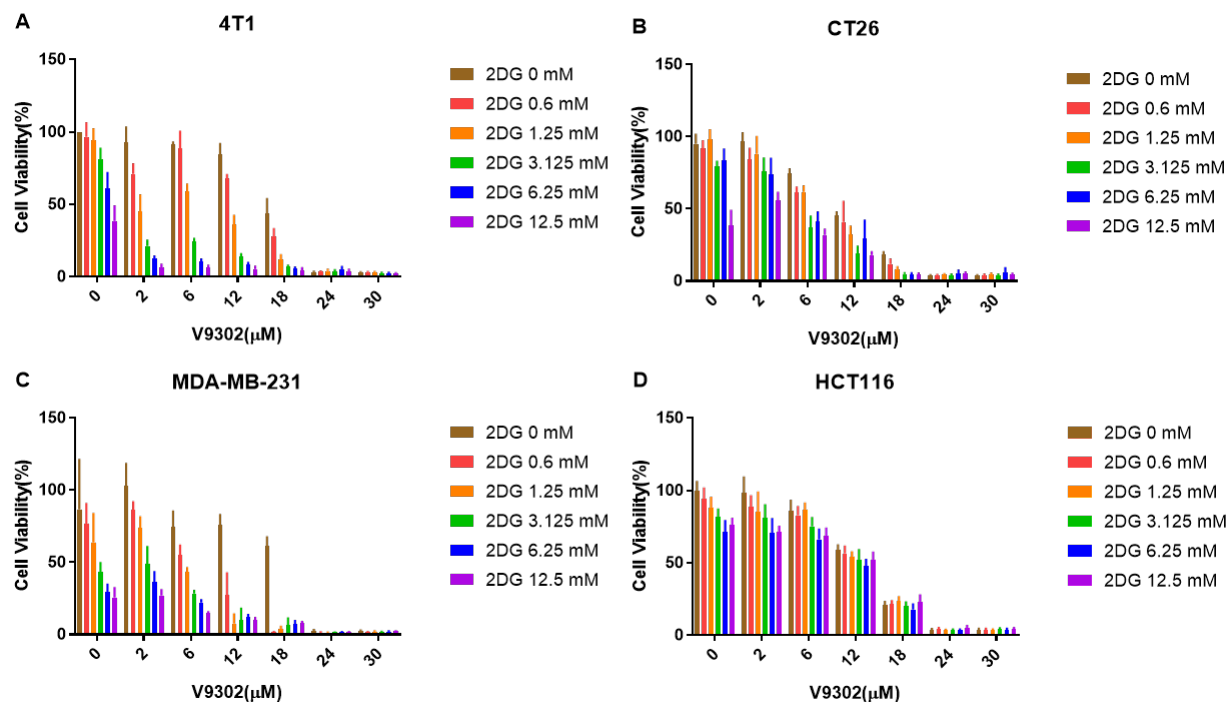


**Figure. 2 Synergistic effect between V9302 and 2-DG in inhibiting the proliferation of different tumor cell lines.**

(A-D) 4T1.2, CT26, MDA-MB-231, HCT116 cells were treated with various concentrations of free V9302 and free DOX or the combination of PPMP and DOX. After 48 h, the cytotoxicity was determined by MTT assay. The experiments were performed in triplicate and repeated three times. Data are presented as means  $\pm$  SD.

**Table. 1 Synergistic Antiproliferative Activity of V9302 and 2-DG in Cancer Cells**

	d1(mM)	D <sub>50</sub> 1 (mM)	d2( $\mu$ M)	D <sub>50</sub> 2( $\mu$ M)	CI
MCF-7	0.6	9.017 $\pm$ 0.78	9.485 $\pm$ 0.89	11.83 $\pm$ 0.75	0.868
MDA-MB-231	0.6	2.649 $\pm$ 0.60	6.437 $\pm$ 0.81	18.64 $\pm$ 0.53	0.572
CT26	0.6	11.05 $\pm$ 1.03	7.661 $\pm$ 0.46	10.09 $\pm$ 0.44	0.816

4T1.2	0.6	3.989±0.53	12.1±0.59	16.79±0.56	0.871
HCT116	0.6	15.47±1.37	11.09±0.41	12.69±0.31	0.913

Combination Index (CI) of simultaneous treatment of V9302 and 2-DG in MCF-7, MDA-MB-231, CT26, 4T1.2, HCT116 cells. Cells were treated with a combination of 2-DG and V9302 and cell viability was determined by MTT assay. The CI was calculated by the formula:  $CI=(d1/D_{501})+(d2/D_{502})$ , where  $D_{501}$  is the concentration of 2-DG required to produce 50% effect alone, and  $d1$  is the concentration of 2-DG required to produce the same 50% effect in combination with  $d2$ .  $D_{502}$  is similarly the concentration of V9302 required to produce 50% effect alone, and  $d2$  is the concentration of V9302 required to produce the same 50% effect in combination with  $d1$ . The CI values are interpreted as follows: <1.0, synergism; 1.0, additive; and >1.0, antagonism. Each experiment was done in triplicate

### 3.2 Synthesis and Characterization of the POEG-p-2DG micelles

The synthesis route of POEG-p-2DG is shown in the synthesis scheme 1. All of the intermediates and final product POEG-p-2DG are confirmed by <sup>1</sup>H-NMR (Fig. S1-S3). The average molecular weight of POEG-p-2DG polymer was determined and calculated by both NMR and gel permeation chromatography. Each POEG-p-2DG molecule contained an average of 8 units of OEG<sub>950</sub> and 21 units of VBSS with 2-DG conjugated.

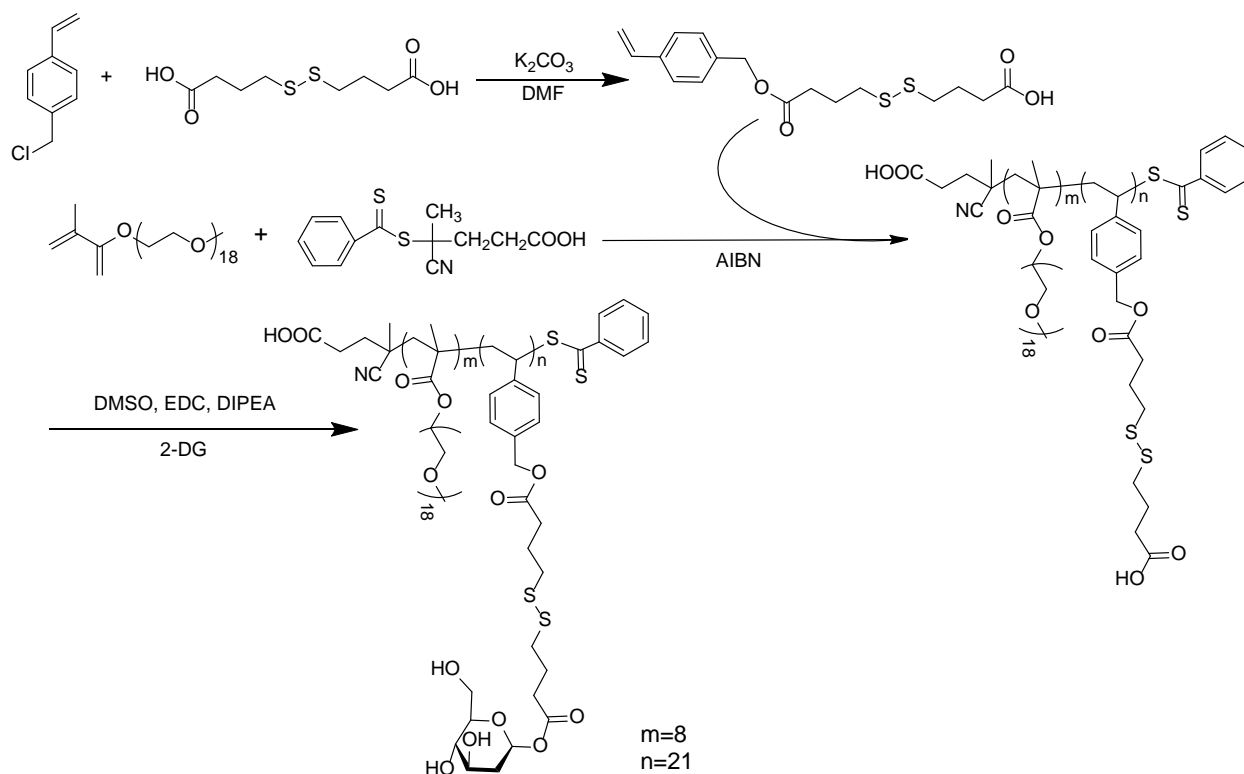


**Figure. 3 Synthesis Scheme of POEG-p-2DG Conjugate**

Blank POEG-p-2DG micelles or V9302-loaded POEG-p-2DG were then prepared by simple film hydration method. The CMC of POEG-p-2DG micelles was determined to be around 0.02mg/mL. The relatively low CMC of POEG-p-2DG shall help to maintain the good stability of the micelles upon being diluted in blood stream after intravenous administration and prevent the early release before reaching to the tumor site. The hydrodynamic sizes of p-VBSS backbone micelles, blank POEG-p-2DG micelles or V9302-loaded POEG-p-2DG micelles were examined by dynamic light scattering as shown in Fig. 4. The polymer backbone POEG-p-VBSS without 2-DG conjugation formed micelles with size around 100nm, which is consistent with previous study (Jingjing Sun, personal communications). However, after the post-conjugation of 2-DG to the polymer backbone, the size of the resulting POEG-p-2DG micelles drastically decreased to around 10-15nm. Loading of V9302 into POEG-p-2DG micelles had minimal impact on the particle size. This might be because the conjugation of highly water-soluble molecule 2-DG increases the

hydrophilicity of the polymer and greatly facilitates the size reduction. TEM further shows that the spherical morphology with homogenous size distribution of both blank POEG-p-2DG or V9302-loaded POEG-p-2DG micelles, which is consistent with the result of DLS analysis.

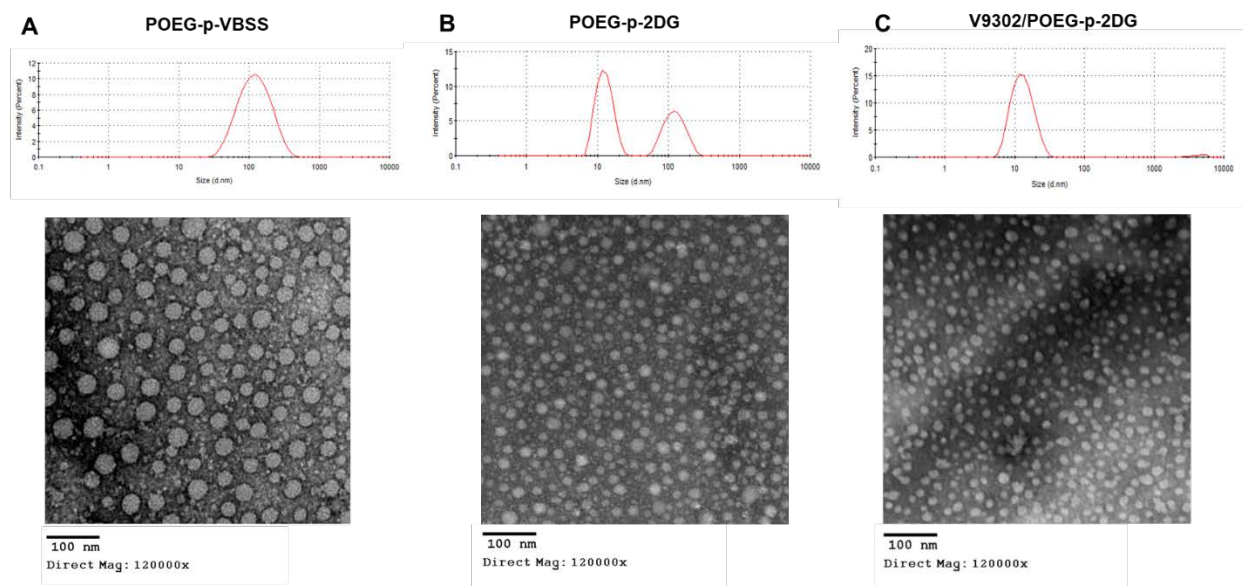


**Figure. 4 DLS and TEM Characterization of (A)POEG-p-VBSS, (B)POEG-p-2DG and (C)V9302-loaded POEG-p-2DG micelles**

Polymer backbone POEG-p-VBSS micelles (A), Blank POEG-p-2DG micelles (B) and V9302-loaded POEG-p-PPPMP micelles (C) using negative staining. V9302 loaded in to POEG-*b*-PPPMP micelles at carrier/drug ratio of 20/1 (mg/mg). Scale bar is 100 nm.

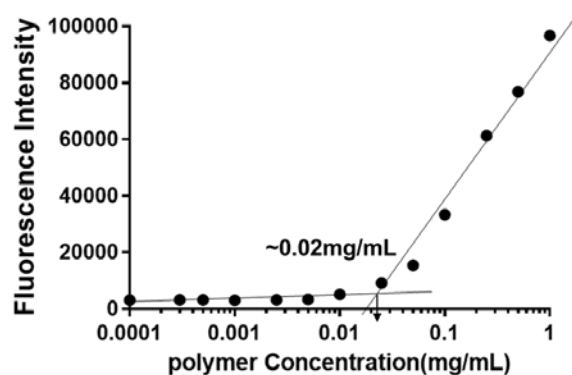


**Figure. 5 Measurement of Critical Micelle Concentration of POEG-p-2DG micelles**

### 3.3 *In vitro* Drug Release Study

The release profile of V9302 from V9302-loaded POEG-p-2DG micelles was investigated by using a dialysis method with PBS containing varying concentrations of GSH (0, 10mM). As shown in Fig. 6, free V9302 was quickly diffused outside the dialysis bag. Around 70% of free V9302 was diffused out rapidly in 2 h and around 90% of V9302 was diffused out from the dialysis bag after 12 h. Meanwhile, the V9302 release from POEG-p-2DG micelles are significantly slower. In the absence of GSH treatment, only less than 20% of V9302 loaded in POEG-p-2DG was released out after 2 h, and the slow kinetics of release was extended for 48 h. However, upon exposure to 10 mM GSH, the release of V9302 from the POEG-p-2DG micelles was greatly accelerated: 20% more V9302 was released compared with the group without GSH. This is likely due to the disassembly of the micelles, which was induced by the cleavage of disulfide link.

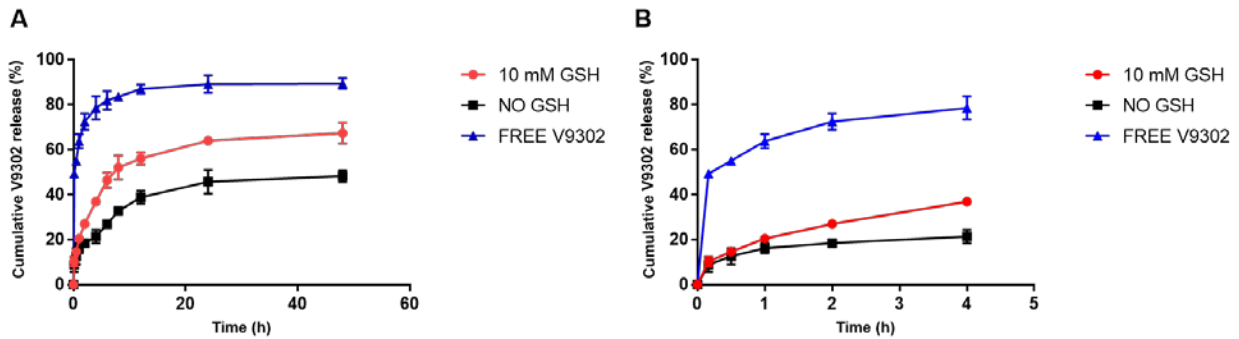


**Figure. 6** Cumulative V9302 release profile from POEG-p-2DG micelles and free V9302 in 48h.

(A) 0 to 48 hours, (B) 0 to 4 hours. PBS was used as the release medium. V9302 concentration was fixed at 6 mg/mL.

Values reported are the means  $\pm$  SD for triplicate samples.

### 3.4 In vitro Cytotoxicity of V9302 loaded POEG-p-2DG Micelles

The *in vitro* cytotoxicity of V9302-loaded POEG-p-2DG micelles (micelles to drug ratio: 20:1 (w/w)) was tested on a broad range of cell lines. As shown in Fig. 7, V9302 inhibited the proliferation of 4T1 cancer cells in a concentration-dependent manner (A). Blank POEG-p-2DG micelles alone also showed modest cytotoxicity towards the cancer cells (A). However, V9302-loaded POEG-p-2DG showed decreased IC<sub>50</sub> when compared to V9302 alone. Similar results were also observed in other types of cell lines (B-E). These data indicated that POEG-p-2DG might sensitize the response of cancer cells towards V9302 and achieve a synergistic effect, which is consistent with data from free drug combination (Fig. 2). This is likely attributed to the release of active 2-DG following the uptake of the micelles and the subsequent cleavage of self-immolative linker, resulting in synergistic interaction with V9302.

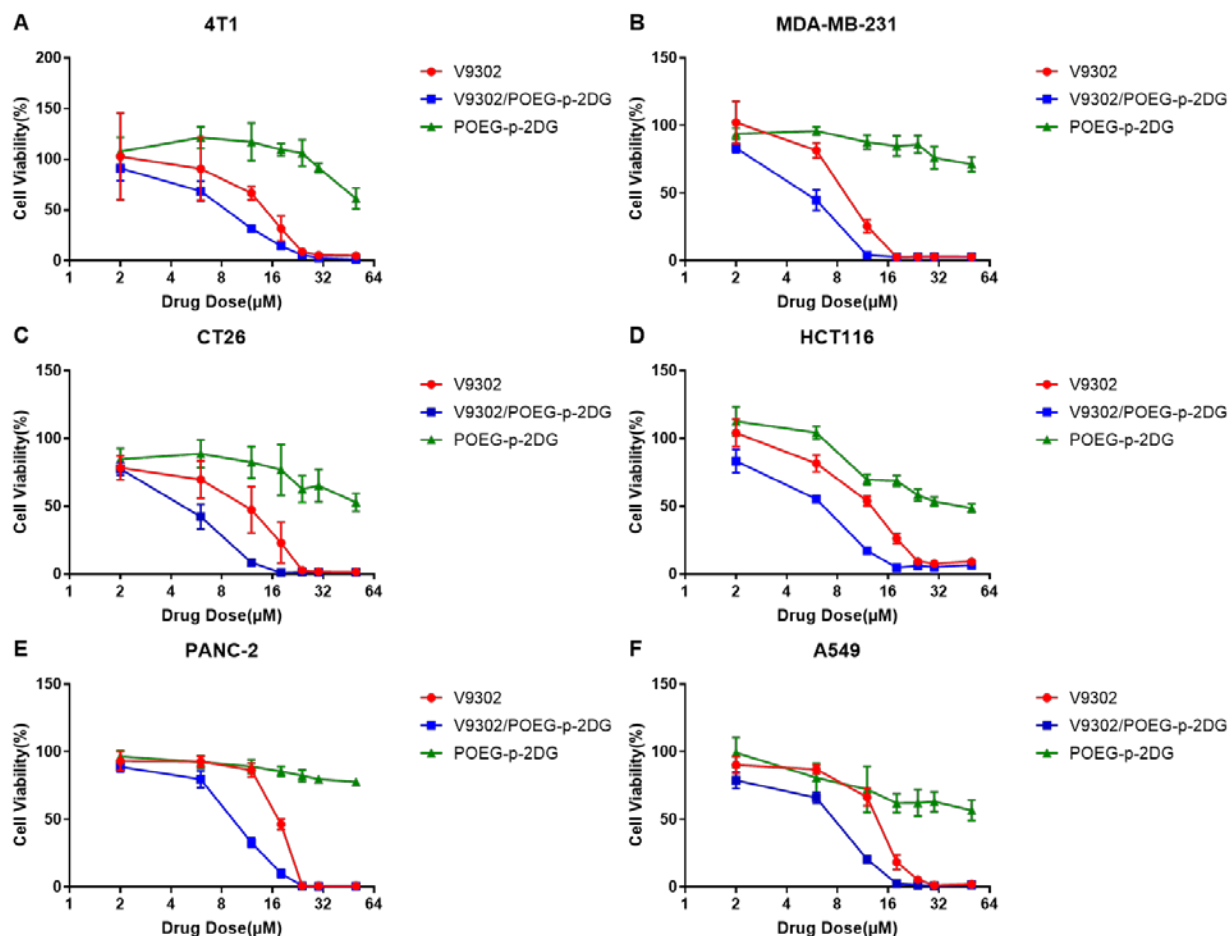


**Figure. 7 Cytotoxicity of POEG-p-2DG and V9302-loaded POEG-p-2DG micelles**

4T1.2 (A), MDA-MB-231 (B), CT26 (C), HCT116 (D), PANC-2 (E) and A549 (F) cell lines after 48 h treatment with V9302, POEG-p-2DG and V9302-loaded POEG-p-2DG. Data are presented as the means  $\pm$  SD for triplicate samples.

### 3.5 Effect of V9302-loaded POEG-p-2DG micelle on glucose and glutamine metabolism

It has been previously reported that the glucose consumption in tumor cells was significantly increased when glutamine metabolism was interfered [27-29]. We also observed a similar increase in glucose uptake after V9302 treatment in both 4T1 and CT26 cell lines. We then went on to examine whether V9302/POEG-p-2DG micelles could block the increased glucose

metabolism induced by V9302. As expected, V9302 treatment led to a significant increase in both glucose uptake and lactate production (Fig. 8). The upregulation in glucose metabolism induced by V9302 was inhibited when V9302 was loaded in POEG-p-2DG micelles. However, POEG-p-2DG itself did not have significant impact on the basal levels of glucose uptake and lactate production. As a positive control, free 2-DG (10 mM) significantly inhibited the lactate production. Treatment with free 2-DG (10 mM) also led to a slight decrease in glucose uptake but this is not statistically significant. The more dramatic effect of POEG-p-2DG micelles on glucose uptake/lactate production upon co-treatment with V9302 might be due to increased susceptibility of the tumor cells to the inhibition by 2-DG when the glucose metabolism was upregulated.

Then glutamine metabolism was examined by measuring glutamine uptake (Fig. 8C). In consistent with previous study, the uptake of glutamine was significantly inhibited by V9302. Interestingly, treatment with V9302/POEG-p-2DG led to a further decrease in glutamine uptake. We also noticed slight decreases in the uptake of glutamine following treatment with POEG-p-2DG or free 2-DG; however, this was not statistically significant. To understand the potential mechanism involved in the impact of POEG-p-2DG or 2-DG on the uptake of V9302, we examined the ASCT2 glycosylation following various treatments as glycosylated ASCT2 is more active than the non-glycosylated counterpart in glutamine transport. As shown in Fig. 8D, significant inhibition of ASCT2 glycosylation was observed following treatment with POEG-p-2DG, V9302/POEG-p-2DG, or free 2-DG, particularly the free 2-DG at a high concentration.

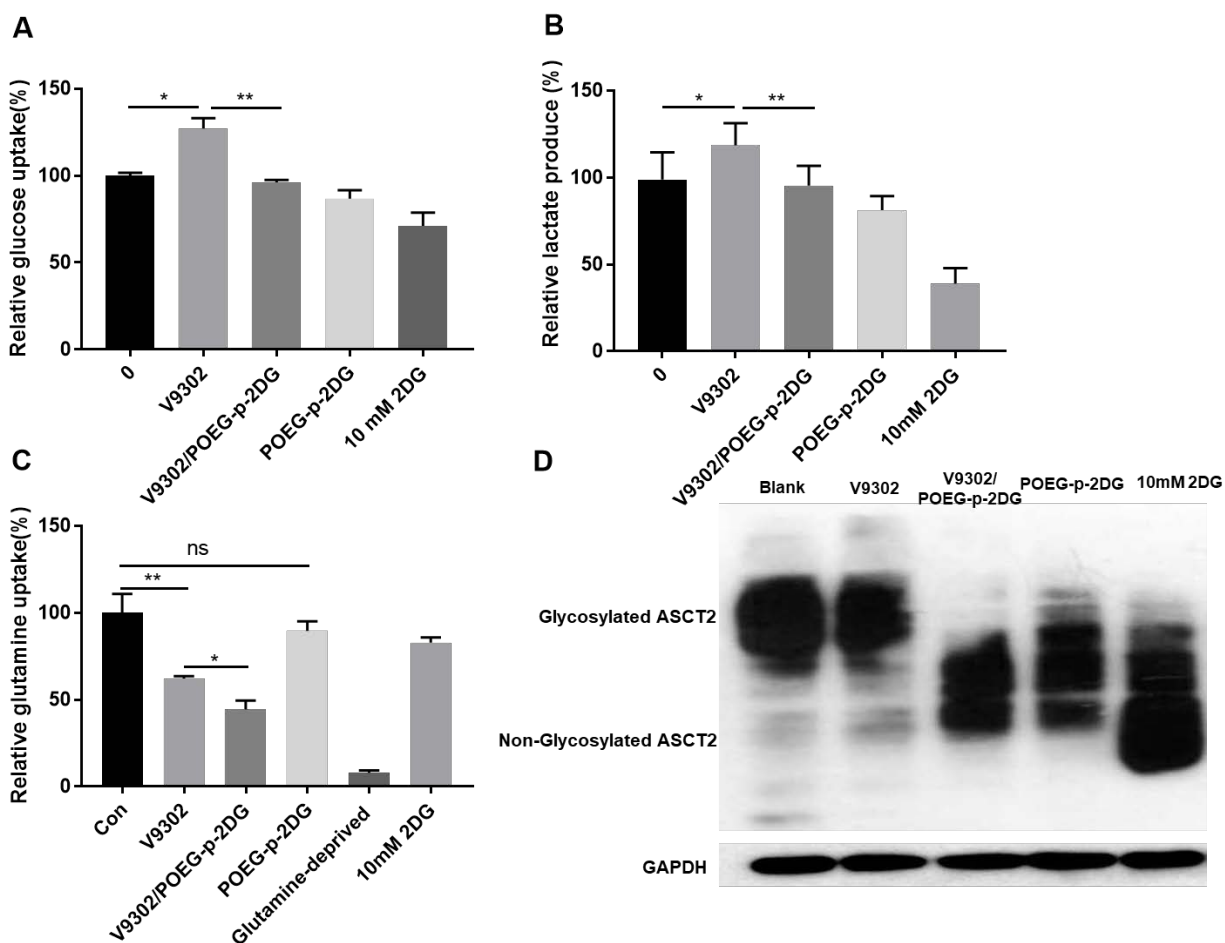


**Figure. 8 V9302/POEG-p-2DG have inhibition effect on both glucose metabolism and glutamine metabolism.** V9302/POEG-p-2DG could downregulate compensatory glucose metabolism from (A) glucose uptake and (B) lactate production. (C) V9302/POEG-p-2DG can further inhibit the glutamine uptake. (D) POEG-p-2DG could downregulate the glycosylation of ASCT2. Data are presented as the means  $\pm$  SD for triplicate samples.

### 3.6 Biodistribution study

The *in vivo* biofluorescence imaging was used for the assessment of the biodistribution of POEG-p-2DG micelles after systemic administration. DiR was loaded into POEG-p-2DG to form mixed micelles with similar size (10-15 nm) and then *i.v.* injected to allow near infrared imaging

of mice with free DiR as a control. Whole body imaging shows that DiR loaded into POEG-p-2DG micelles was mainly concentrated at tumor site while free DiR was largely found in the area of liver (Fig. 9A). Fig. 9B shows the ex vivo imaging of tumors and other major organs that were removed from the mice after the completion of whole-body imaging. In consistent with whole body imaging, strong signals were observed in tumor tissues, significantly higher than those in other normal organs and tissues. We also observed significant uptake of the nanoparticles by liver and spleen. The fluorescence signals in tumors and other organs were significantly lower following injection of free DiR. In addition, the signals were mainly concentrated in the liver. These data suggest that free DiR was quickly eliminated while the DiR loaded into POEG-p-2DG micelle exhibited extended half-life in the circulation. (Fig. 9 C, D)

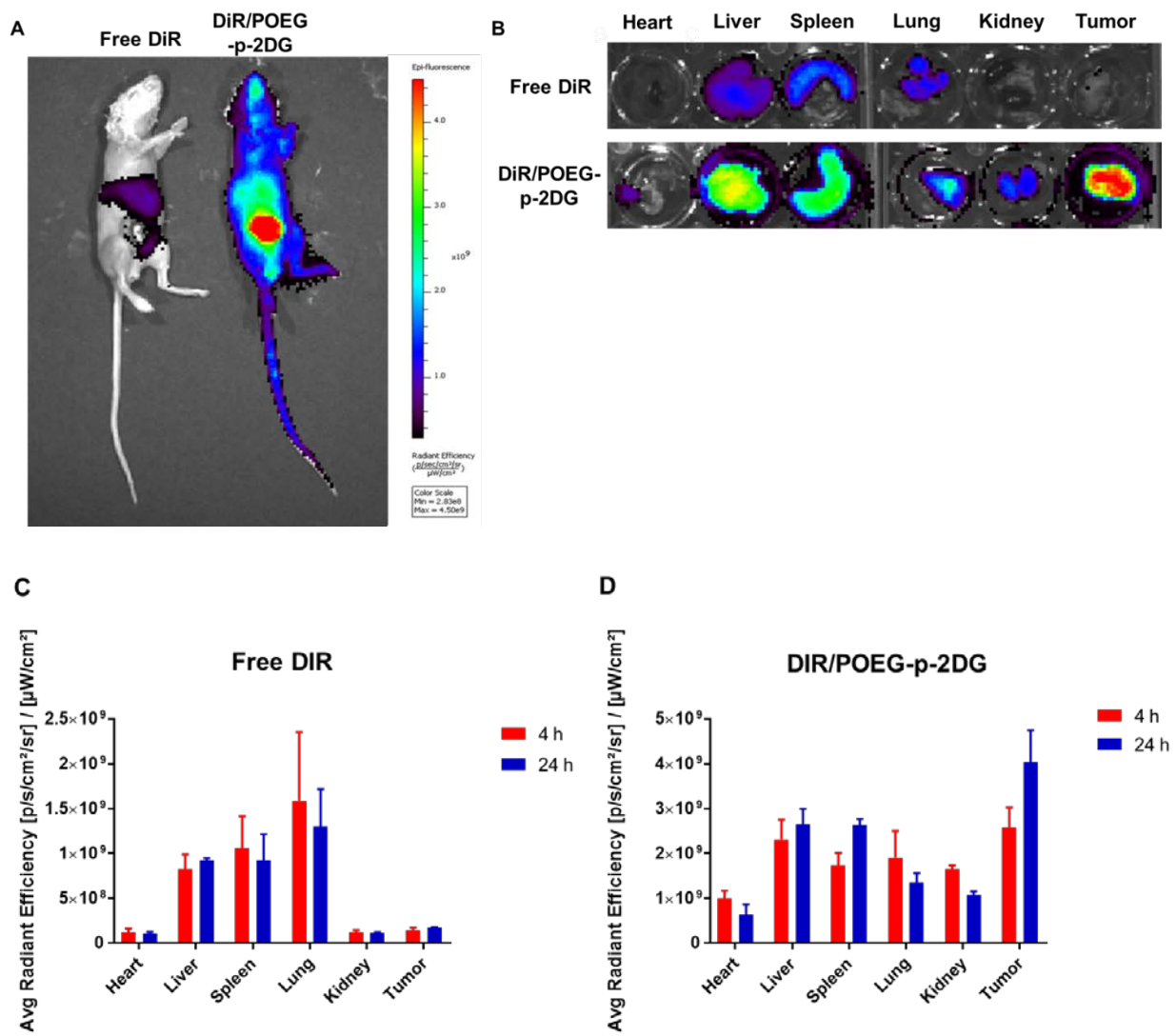


**Figure. 9 In vivo(A) and ex vivo(B-D) of NIRF imaging of biodistribution of POEG-p-2DG formulation**

(A) The whole-body fluorescence image at 24 h after intravenously injection of free DiR and DiR loaded in POEG-p-2DG micelle. (B) The organ fluorescence image at 24 h after intravenously injection of free DiR and DiR loaded in POEG-p-2DG micelle. (C-D) Quantified fluorescence intensity of different organ at 4h and 24h after intravenously injection of free DiR and DiR loaded in POEG-p-2DG micelle.

### 3.7 In vivo Therapeutic and Toxicological Study

The in vivo tumor growth inhibitory activity of V9302/POEG-p-2DG was investigated in a highly aggressive syngeneic murine breast cancer model 4T1.2 (s.c. at mammary fat pad). Blank POEG-p-2DG showed minimal antitumor activity, this might be due to the limited dose of POEG-p-2DG that was used to deliver V9302. i.v. injection of V9302 and 2-DG in combination also exhibited limited improvement of antitumor efficacy. i.p injection of V9302 alone showed modest antitumor efficacy and combination of V9302 with 2-DG via i.p. route led to an enhancement in antitumor activity although it was not statistically significant. Among all treatment groups, V9302/POEG-p-2DG group was most effective in inhibiting the tumor growth. The weights and images of tumor tissue that were collected at the end of the experiment were shown in Fig. 10 B and Fig. 10 C, respectively, which was consistent with data of tumor growth curves. Also, the ki67 staining further confirm the tumor growth inhibition effect of V9302/POEG-p-2DG micelles. (Fig. 11)

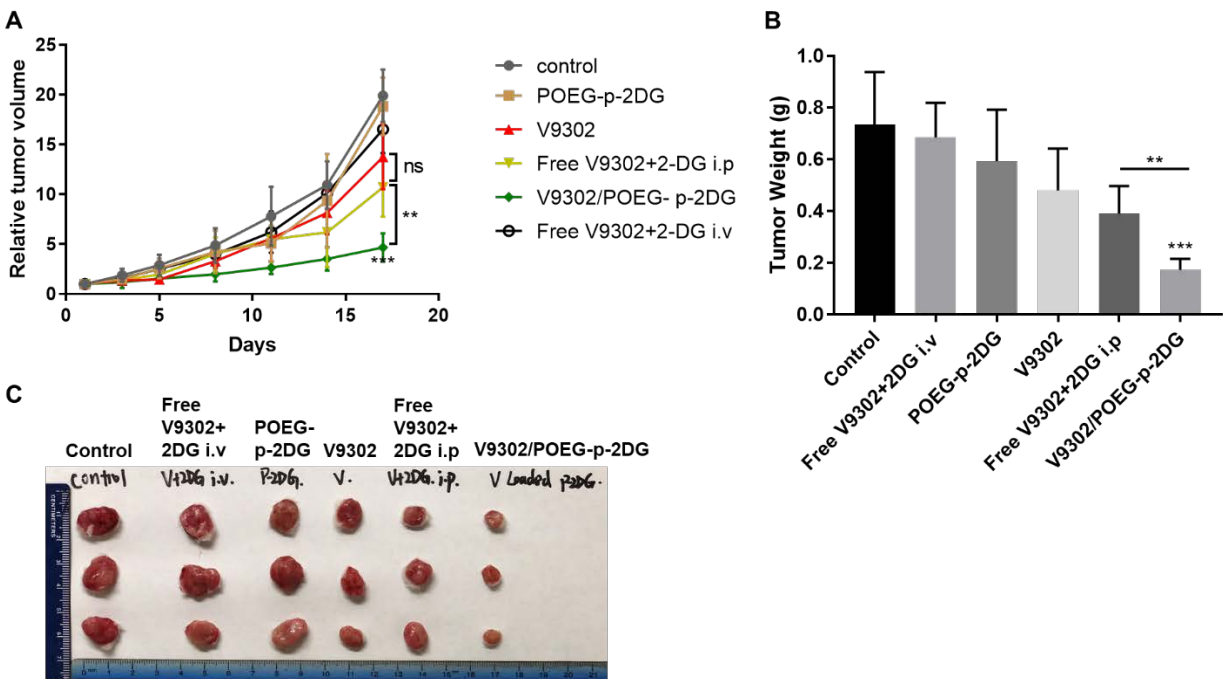


**Figure. 10 Enhanced in vivo antitumor activity of V9302-loaded POEG-p-2DG micelle**

Blank POEG-p-2DG micelles, V9302, Free drug combination of V9302 and 2-DG via i.p or i.v injection and V9302 loaded POEG-p-2DG micelles in a syngeneic murine breast cancer model (4T1.2). Five injections were given on day 1, 3, 5, 8 and 11. (B) Weights of tumors collected from different groups at the end of experiment. (C) Photographs of tumors collected from different treatment groups at the end of experiment. Values reported are the means  $\pm$  SEM, n = 5. P values were generated by one-way ANOVA using the Tukey test for multiple comparisons. \*P < 0.05, \*\*P < 0.01, \*\*\*P < 0.001 (vs control).

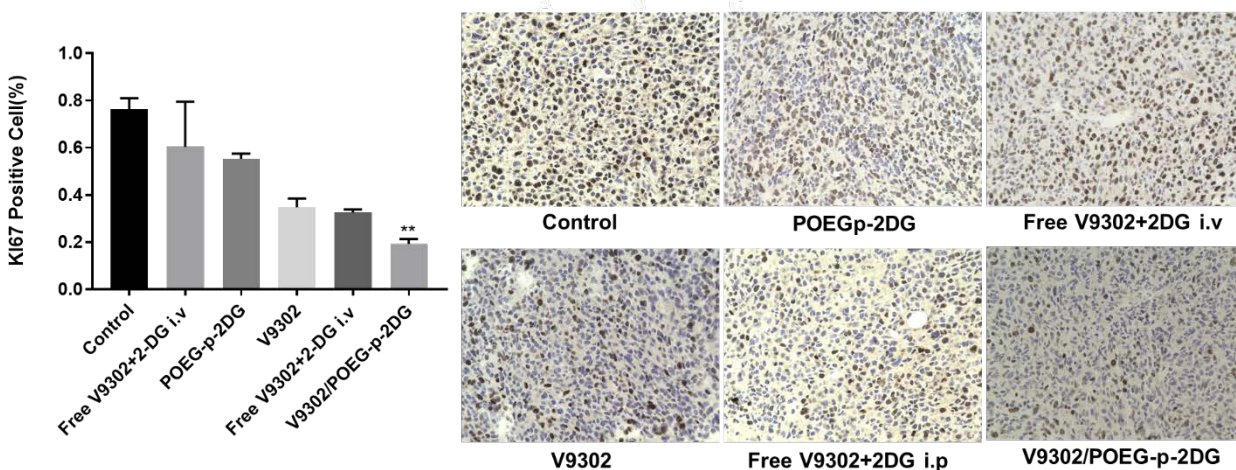


**Figure. 11 Histological analysis of tumor tissues by ki67 staining**

Tissue were collected from different groups at the end of in vivo therapeutic experiment using ki67 staining. Ki 67 positive cells were quantified by using ImageJ software.

Body weights were also monitored together with the tumor growth (Fig. 12A). Treatment with blank POEG-p-2DG or V9302/POEG-p-2DG had no obvious effect on body weights compared to control group. However, significant decreases in body weights were observed in mice treated with V9302&2-DG free drug combination via i.p. route. We also noticed significant decreases in body weights after three injections of V9302&2-DG free drug combination via i.v. route. But, after increasing the injection interval, the body weights of these mice grew back to normal range while the body weights continued to decrease in mice receiving combination

treatment via i.p. injection. Serum levels of ALT/AST and creatinine were also measured to further evaluate the toxicity. As shown in Fig. 12, there were significant increases in the serum levels of ALT/AST following the free drug combination treatment via i.p route. In contrast, treatment with V9302/POEG-p-2DG showed minimal effects on the levels of the transaminases. No significant increases in serum levels of were observed in any of the treatment groups. These results indicated that V9302/2-DG combination may lead to liver toxicity while V9302/POEG-p-2DG formulation was well-tolerated at the doses used.

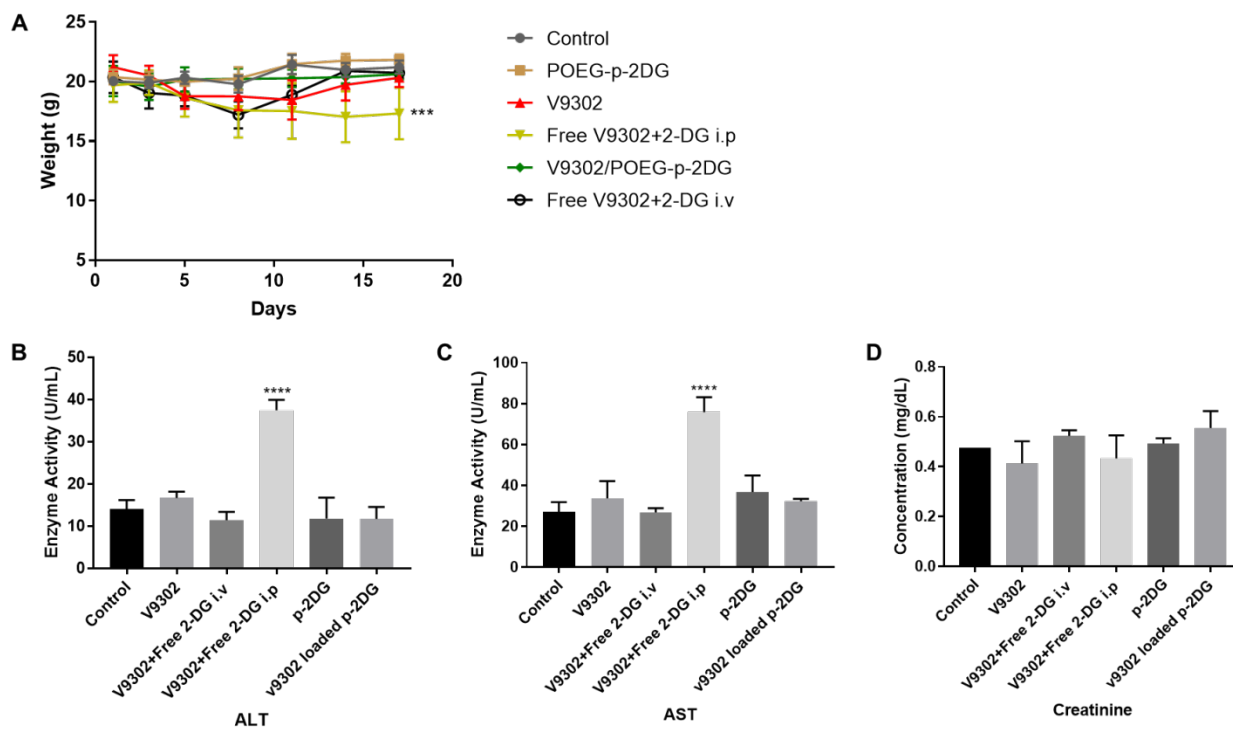


**Figure. 12 Toxicological assay of V9302-loaded POEG-p-2DG micelle**

Toxicity assay of blank POEG-p-2DG micelles, V9302, Free drug combination of V9302 and 2-DG via i.p or i.v injection and V9302 loaded POEG-p-2DG micelles in a syngeneic murine breast cancer model (4T1.2). (A) Changes of body weight in mice receive different treatment. (B-D) ALT, AST and creatinine assay of serum collected from different groups at the end of in vivo therapeutic experiment.

## 4.0 Discussion

The reprogrammed metabolic pathway that cancer cells depend on suggests an opportunity for cancer targeted therapy and precision medicine[31]. It is well known the energy production in cancer cell uniquely demands on specific nutrients, such as glucose and glutamine. Despite increasing evidence that demonstrates the prominent role of reprogrammed glycolysis and glutaminolysis in cancer cell growth, homeostasis and tumor microenvironment maintenance, still no single agent based on glucose or glutamine metabolism is likely to control tumor growth effectively[32]. One possible reason is the complicated metabolic metabolism networking resulting in compensating mechanism between glucose, glutamine or other pathways that undermine the efficacy of monotherapy based on cancer metabolism[28, 33]. Therefore, combination therapy with a focus on inhibition of multiple metabolic pathways might be a better strategy than trying to administer maximum tolerated doses of metabolic drugs that are targeted at a single pathway.

V9302 is a selective and potent small molecule antagonist of glutamine transporter ASCT2, which was shown to have significant impact on glutamine metabolism and tumor growth. However, its poor aqueous solubility may hinder its clinical development. Also, in consistent with previous reports[27-29], we overserved that inhibition of glutamine metabolism by V9302 results in compensatory upregulation of glucose metabolism, such as increases in glucose uptake (Fig. 8) and the mRNA expression levels of several glucose metabolism-related genes. Hence, combination of V9302 with an inhibitor of glycolysis shall represent an effective strategy to improve the therapeutic outcome.

2-DG is a glucose analog that is widely used for glycolysis inhibition. Our study showed a synergistic effect with the combination of V9302, which might be attributed to the blockade of the compensatory upregulation of glucose metabolism induced by V9302 treatment. The underlying mechanism for the compensatory metabolic reprogramming is still unclear and requires more studies in the future. Interestingly, besides glucose metabolism inhibition, 2-DG appear to be able to further decrease the glutamine uptake when combined with V9302. One of the possible mechanisms is that 2-DG can block the glycolysis pathway, which can further interfere with the glycosylation process of ASCT2. Without sufficient glycosylation, the glutamine uptake function of ASCT2 is likely to be undermined[34]. Nonetheless, the inhibition of glutamine uptake that was brought by 2-DG was only observed in the presence of V9302 co-treatment. This might be due to the fact that the decreased glycosylation following 2-DG treatment alone is not sufficient to compromise the glutamine uptake due to the existence of compensatory mechanisms such as upregulation of ASCT2 expression [33, 34]. On the other hand, inhibition of ASCT2 by V9302 may lead to sensitization of cells to 2-DG treatment with respect to its impact on glutamine uptake through inhibition of ASCT2 glycosylation.

Recently, nanocarriers have been employed to improve the delivery of metabolism inhibitors to tumors to improve the efficacy and decrease the toxicity. Amira Elgogary et al. reported the use of PEG-PLGA nanoparticle for the delivery of BETES, a prototype GLS1 inhibitor. Moreover, further improvement in antitumor efficacy was demonstrated in combination with free metformin that inhibits glycolysis [26]. However, no reports have been published on codelivery of glucose and glutamine inhibitors to tumors. It has been challenging to co-formulate the two different inhibitors as one is often water soluble and the other one is water insoluble.

As a strategy to facilitate the co-delivery of the highly water-soluble 2-DG and the hydrophobic compound V9302, we have developed a 2-DG prodrug-based dual-functional polymeric carrier, POEG-p-2DG that is capable of codelivery of V9302. One common issue with pro-drug carrier is the release of the original drug from the conjugated polymer. In this study, we introduce 4,4'-dithiodibutyric acid as the self-immolative linker between 2-DG and polymer backbone to facilitate the redox-responsive release of 2-DG in the cytoplasm. Moreover, this hydrophobic link could also support the hydrophobic interaction to facilitate the loading of V9302. POEG-p-2DG could readily form micelles via a simple film hydration method. Interestingly, coupling of 2-DG to the polymer backbone led to a drastic decrease in the particle size from 100 to 15 nm. Loading of V9302 into the micelles had minimal impact on the particle size. The ultra-small sizes shall facilitate the micelle penetration to hypoxic core of tumor[35]. Interestingly, tumor cells in the hypoxic environment might have better response to 2-DG due to increased dependency on anaerobic glycolysis[36], which warrants more studies in the future.

POEG-p-2DG retains the pharmacological activity of free 2-DG as evident from its activity in inhibiting basal level of glucose metabolism and in reversing the V9302-induced upregulation of glucose metabolism. More importantly, POEG-p-2DG could also inhibit glycosylation of ASCT2 and further decrease the glutamine uptake when combined with V9302. The more dramatic impact of POEG-p-2DG on glucose or glutamine metabolism that is seen in presence of V9302 co-treatment might be due to sensitization of tumor cells to POEG-p-2DG treatment when the function of ASCT2 is inhibited.

POEG-p-2DG-formulated V9302 demonstrated significantly enhanced antitumor activity both *in vitro* and *in vivo*. Particularly, codelivery of V9302 via POEG-p-2DG led to effective growth inhibition of tumor in an aggressive murine breast cancer model (4T1.2), much more

effectively than V9302 monotherapy or V9302&2-DG free drug combination. 2-DG could be effectively released from POEG-p-2DG following delivery to tumor cells and the synergistic effect between the released 2-DG and V9302 shall contribute to the improved antitumor activity. The improved delivery of both 2-DG and V9302 via POEG-p-2DG nanocarrier shall also play an important role. In addition to improved antitumor activity, codelivery of 2-DG and V9302 via POEG-p-2DG overcame the systemic toxicity that is associated with free drug combination. This will allow the use of a higher drug dose to maximize the therapeutic effect.

### Conclusion

We have developed a well-characterized POEG-p-2DG prodrug-based micellar nanocarrier for efficient delivery of V9302, a water-insoluble inhibitor of glutamine uptake transporter. POEG-p-2DG well retained the pharmacological activity of 2-DG. V9302 loaded in POEG-p-2DG micelles exhibited slow release kinetics *in vitro*. Combination of V9302 with POEG-p-2DG led to inhibition of the compensatory metabolic shift to glucose metabolism that was induced by V9302 treatment. It also led to more effective inhibition of glutamine uptake likely due to POEG-p-2DG-mediated inhibition of ASCT2 glycosylation. V9302/POEG-p-2DG showed more cytotoxicity towards cultured cancer cells than V9302 alone. More importantly, systemic administration of V9302 formulated in POEG-p-2DG micelles resulted in significantly improved antitumor activity as well as decreased systemic toxicity.

## Appendix A Supplementary Materials

### A.1 $^1\text{H-NMR}$

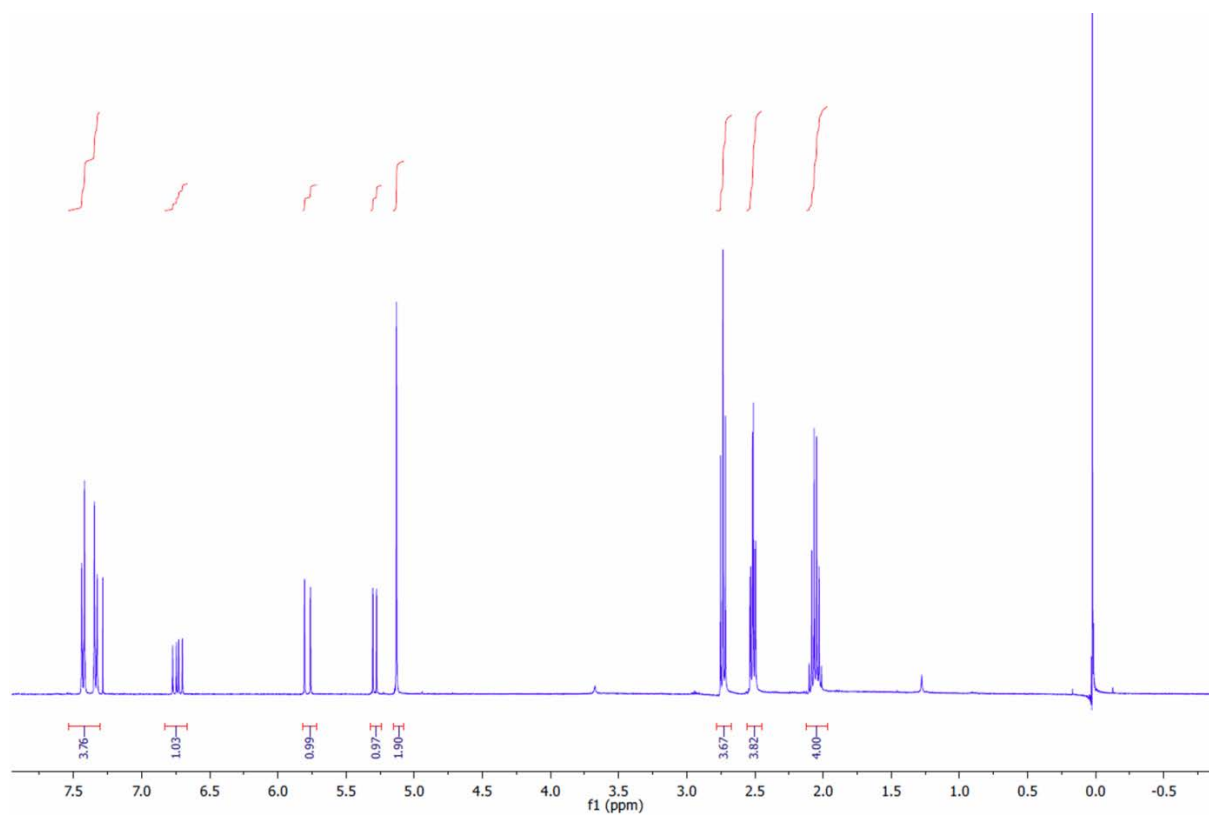


Figure S 1  $^1\text{H-NMR}$  of VBSS monomer

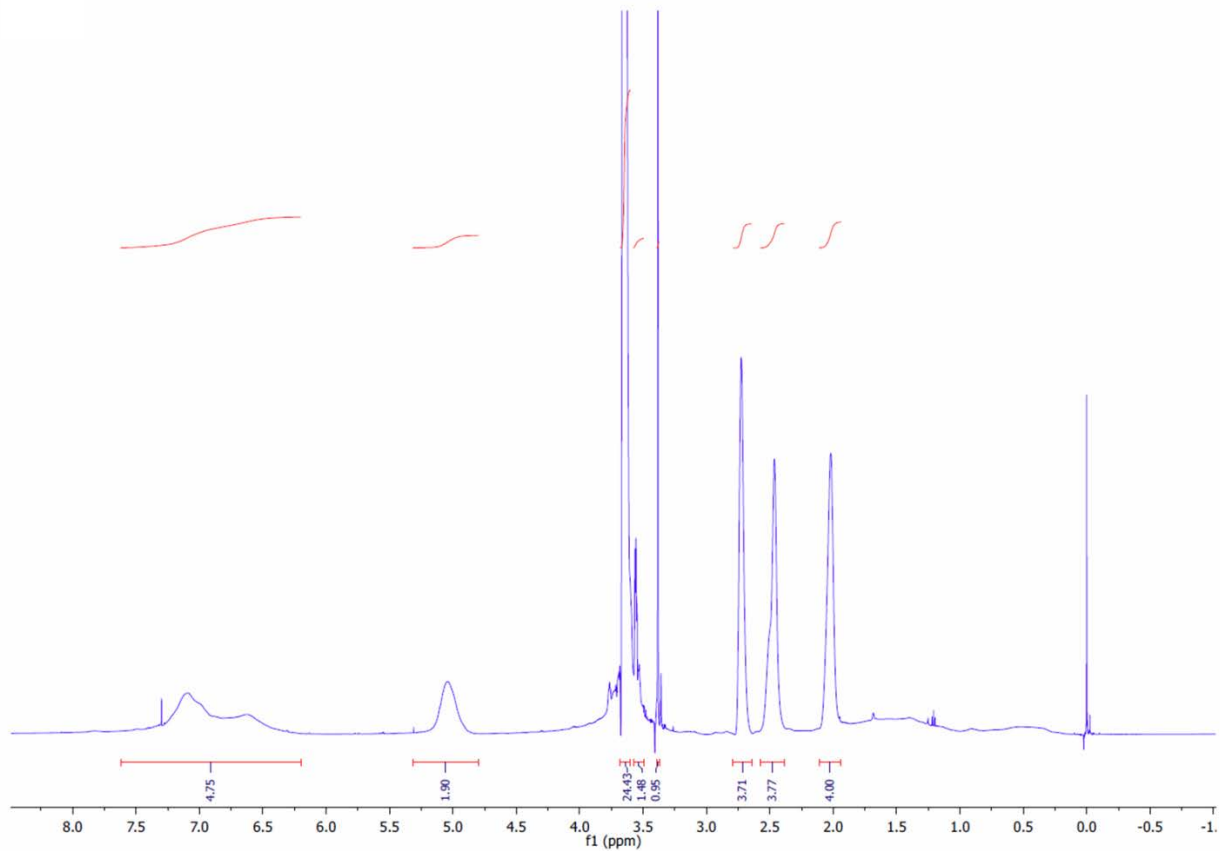
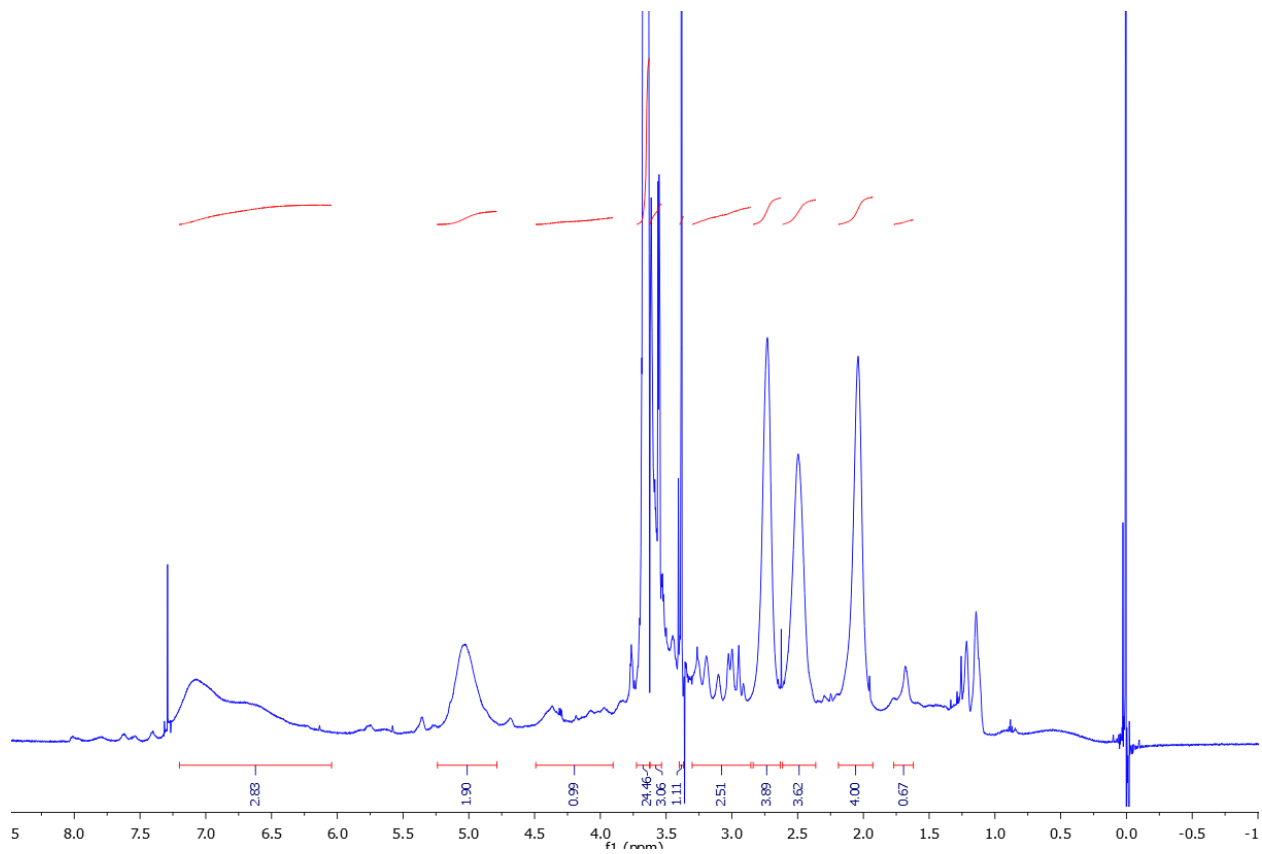
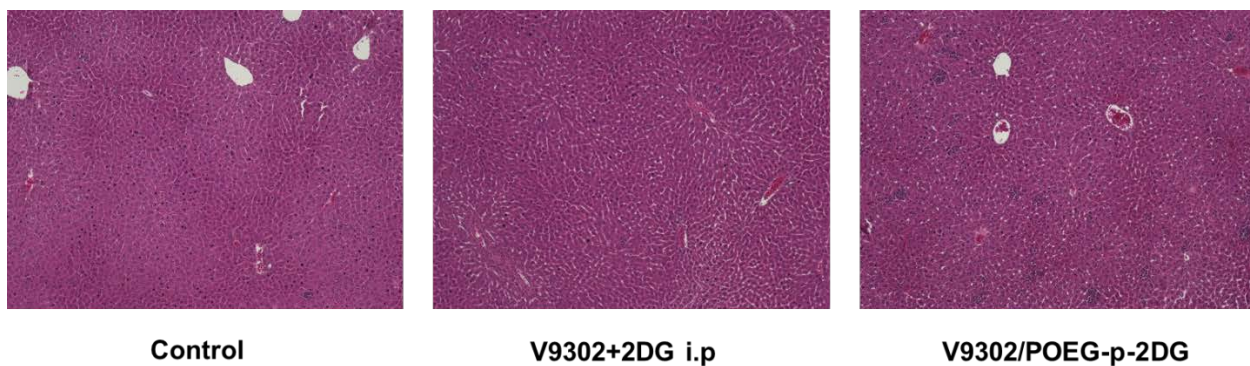


Figure S 2 <sup>1</sup>H-NMR of POEG-p-VBSS polymer backbone



**Figure S 3  $^1\text{H-NMR}$  of POEG-p-2DG**

### **A.2 H&E staining of liver**



**Figure S 4 H&E staining of liver**

## Bibliography

- [1] N. Hay, Reprogramming glucose metabolism in cancer: can it be exploited for cancer therapy?, *Nat Rev Cancer* 16(10) (2016) 635-49.
- [2] M.G. Vander Heiden, Targeting cancer metabolism: a therapeutic window opens, *Nat Rev Drug Discov* 10(9) (2011) 671-84.
- [3] B. Smith, Xenia L. Schafer, A. Ambeskovic, Cody M. Spencer, H. Land, J. Munger, Addiction to Coupling of the Warburg Effect with Glutamine Catabolism in Cancer Cells, *Cell Reports* 17(3) (2016) 821-836.
- [4] D.A. Tennant, R.V. Durán, E. Gottlieb, Targeting metabolic transformation for cancer therapy, *Nature Reviews Cancer* 10 (2010) 267.
- [5] R.J. DeBerardinis, J.J. Lum, G. Hatzivassiliou, C.B. Thompson, The Biology of Cancer: Metabolic Reprogramming Fuels Cell Growth and Proliferation, *Cell Metabolism* 7(1) (2008) 11-20.
- [6] M.G. Vander Heiden, L.C. Cantley, C.B. Thompson, Understanding the Warburg Effect: The Metabolic Requirements of Cell Proliferation, *Science* 324(5930) (2009) 1029.
- [7] O. Warburg, On the Origin of Cancer Cells, *Science* 123(3191) (1956) 309.
- [8] H. Pelicano, D.S. Martin, R.H. Xu, P. Huang, Glycolysis inhibition for anticancer treatment, *Oncogene* 25 (2006) 4633.
- [9] J.-H. Cheong, E.S. Park, J. Liang, J.B. Dennison, D. Tsavachidou, C. Nguyen-Charles, K. Wa Cheng, H. Hall, D. Zhang, Y. Lu, M. Ravoori, V. Kundra, J. Ajani, J.-S. Lee, W. Ki Hong, G.B. Mills, Dual Inhibition of Tumor Energy Pathway by 2-Deoxyglucose and Metformin Is Effective against a Broad Spectrum of Preclinical Cancer Models, *Molecular Cancer Therapeutics* 10(12) (2011) 2350.
- [10] A.E. Papatianassiu, N.J. MacDonald, D.R. Emler, H.A. Vu, Antitumor activity of efrapetins, alone or in combination with 2-deoxyglucose, in breast cancer in vitro and in vivo, *Cell Stress and Chaperones* 16(2) (2011) 181-193.
- [11] G. Maschek, N. Savaraj, W. Priebe, P. Braunschweiger, K. Hamilton, G.F. Tidmarsh, L.R. De Young, T.J. Lampidis, 2-Deoxy-glucose Increases the Efficacy of Adriamycin and Paclitaxel in Human Osteosarcoma and Non-Small Cell Lung Cancers In Vivo, *Cancer Research* 64(1) (2004) 31.
- [12] B. Dwarakanath, D. Singh, A. Banerji, R. Sarin, N. Venkataramana, R. Jalali, P. Vishwanath, B. Mohanti, R. Tripathi, V. Kalia, V. Jain, Clinical studies for improving radiotherapy with 2-deoxy-D-glucose: Present status and future prospects, *Journal of Cancer Research and Therapeutics* 5(9) (2009) 21-26.
- [13] D. Singh, A.K. Banerji, B.S. Dwarakanath, R.P. Tripathi, J.P. Gupta, T.L. Mathew, T. Ravindranath, V. Jain, Optimizing Cancer Radiotherapy with 2-Deoxy-D-Glucose, *Strahlentherapie und Onkologie* 181(8) (2005) 507-514.
- [14] B.K. Mohanti, G.K. Rath, N. Anantha, V. Kannan, B.S. Das, B.A.R. Chandramouli, A.K. Banerjee, S. Das, A. Jena, R. Ravichandran, U.P. Sahi, R. Kumar, N. Kapoor, V.K. Kalia, B.S. Dwarakanath, V. Jain, Improving cancer radiotherapy with 2-deoxy-d-glucose: phase I/II clinical trials on human cerebral gliomas, *International Journal of Radiation Oncology\*Biophysics* 35(1) (1996) 103-111.

- [15] L.E. Raez, K. Papadopoulos, A.D. Ricart, E.G. Chiorean, R.S. DiPaola, M.N. Stein, C.M. Rocha Lima, J.J. Schlesselman, K. Tolba, V.K. Langmuir, S. Kroll, D.T. Jung, M. Kurtoglu, J. Rosenblatt, T.J. Lampidis, A phase I dose-escalation trial of 2-deoxy-d-glucose alone or combined with docetaxel in patients with advanced solid tumors, *Cancer Chemotherapy and Pharmacology* 71(2) (2013) 523-530.
- [16] D. Zhang, J. Li, F. Wang, J. Hu, S. Wang, Y. Sun, 2-Deoxy-D-glucose targeting of glucose metabolism in cancer cells as a potential therapy, *Cancer Letters* 355(2) (2014) 176-183.
- [17] B.J. Altman, Z.E. Stine, C.V. Dang, From Krebs to clinic: glutamine metabolism to cancer therapy, *Nat Rev Cancer* 16(10) (2016) 619-34.
- [18] M. van Geldermalsen, Q. Wang, R. Nagarajah, A.D. Marshall, A. Thoeng, D. Gao, W. Ritchie, Y. Feng, C.G. Bailey, N. Deng, K. Harvey, J.M. Beith, C.I. Selinger, S.A. O'Toole, J.E. Rasko, J. Holst, ASCT2/SLC1A5 controls glutamine uptake and tumour growth in triple-negative basal-like breast cancer, *Oncogene* 35(24) (2016) 3201-8.
- [19] C.T. Hensley, A.T. Wasti, R.J. DeBerardinis, Glutamine and cancer: cell biology, physiology, and clinical opportunities, *J Clin Invest* 123(9) (2013) 3678-84.
- [20] C.V. Dang, J.-w. Kim, P. Gao, J. Yustein, The interplay between MYC and HIF in cancer, *Nature Reviews Cancer* 8 (2008) 51.
- [21] L. Wang, J.J. Li, L.Y. Guo, P. Li, Z. Zhao, H. Zhou, L.J. Di, Molecular link between glucose and glutamine consumption in cancer cells mediated by CtBP and SIRT4, *Oncogenesis* 7(3) (2018) 26.
- [22] R.J. DeBerardinis, A. Mancuso, E. Daikhin, I. Nissim, M. Yudkoff, S. Wehrli, C.B. Thompson, Beyond aerobic glycolysis: Transformed cells can engage in glutamine metabolism that exceeds the requirement for protein and nucleotide synthesis, *Proceedings of the National Academy of Sciences* 104(49) (2007) 19345.
- [23] Y.D. Bhutia, E. Babu, S. Ramachandran, V. Ganapathy, Amino Acid Transporters in Cancer and Their Relevance to "Glutamine Addiction": Novel Targets for the Design of a New Class of Anticancer Drugs, *Cancer Research* 75(9) (2015) 1782.
- [24] Y.-K. Choi, K.-G. Park, Targeting Glutamine Metabolism for Cancer Treatment, *Biomolecules & therapeutics* 26(1) (2018) 19-28.
- [25] M.I. Gross, S.D. Demo, J.B. Dennison, L. Chen, T. Chernov-Rogan, B. Goyal, J.R. Janes, G.J. Laidig, E.R. Lewis, J. Li, A.L. MacKinnon, F. Parlati, M.L.M. Rodriguez, P.J. Shwonek, E.B. Sjogren, T.F. Stanton, T. Wang, J. Yang, F. Zhao, M.K. Bennett, Antitumor Activity of the Glutaminase Inhibitor CB-839 in Triple-Negative Breast Cancer, *Molecular Cancer Therapeutics* 13(4) (2014) 890.
- [26] J.J. Harding, M.L. Telli, P.N. Munster, M.H. Le, C. Molineaux, M.K. Bennett, E. Mittra, H.A. Burris, A.S. Clark, M. Dunphy, F. Meric-Bernstam, M.R. Patel, A. DeMichele, J.R. Infante, Safety and tolerability of increasing doses of CB-839, a first-in-class, orally administered small molecule inhibitor of glutaminase, in solid tumors, *Journal of Clinical Oncology* 33(15\_suppl) (2015) 2512-2512.
- [27] M.L. Schulte, A. Fu, P. Zhao, J. Li, L. Geng, S.T. Smith, J. Kondo, R.J. Coffey, M.O. Johnson, J.C. Rathmell, J.T. Sharick, M.C. Skala, J.A. Smith, J. Berlin, M.K. Washington, M.L. Nickels, H.C. Manning, Pharmacological blockade of ASCT2-dependent glutamine transport leads to antitumor efficacy in preclinical models, *Nat Med* 24(2) (2018) 194-202.
- [28] A. Elgogary, Q. Xu, B. Poore, J. Alt, S.C. Zimmermann, L. Zhao, J. Fu, B. Chen, S. Xia, Y. Liu, M. Neisser, C. Nguyen, R. Lee, J.K. Park, J. Reyes, T. Hartung, C. Rojas, R. Rais, T. Tsukamoto, G.L. Semenza, J. Hanes, B.S. Slusher, A. Le, Combination therapy with BPTES

nanoparticles and metformin targets the metabolic heterogeneity of pancreatic cancer, *Proceedings of the National Academy of Sciences* 113(36) (2016) E5328.

[29] E. Vernucci, V. Gunda, S. Shukla, P.K. Singh, Abstract 3542: Coordination of glutamine and glucose metabolism in pancreatic cancer, *Cancer Research* 77(13 Supplement) (2017) 3542.

[30] M.L. Schulte, A.B. Khodadadi, M.L. Cuthbertson, J.A. Smith, H.C. Manning, 2-Amino-4-bis(aryloxybenzyl)aminobutanoic acids: A novel scaffold for inhibition of ASCT2-mediated glutamine transport, *Bioorganic & Medicinal Chemistry Letters* 26(3) (2016) 1044-1047.

[31] N.S. Akins, T.C. Nielson, H.V. Le, Inhibition of Glycolysis and Glutaminolysis: An Emerging Drug Discovery Approach to Combat Cancer, *Current topics in medicinal chemistry* 18(6) (2018) 494-504.

[32] U.E. Martinez-Outschoorn, M. Peiris-Pagés, R.G. Pestell, F. Sotgia, M.P. Lisanti, Cancer metabolism: a therapeutic perspective, *Nature Reviews Clinical Oncology* 14 (2016) 11.

[33] L. Sun, Y. Yin, L.H. Clark, W. Sun, S.A. Sullivan, A.-Q. Tran, J. Han, L. Zhang, H. Guo, E. Madugu, T. Pan, A.L. Jackson, J. Kilgore, H.M. Jones, T.P. Gilliam, C. Zhou, V.L. Bae-Jump, Dual inhibition of glycolysis and glutaminolysis as a therapeutic strategy in the treatment of ovarian cancer, *Oncotarget* 8(38) (2017) 63551-63561.

[34] F. Polet, R. Martherus, C. Corbet, A. Pinto, O. Feron, Inhibition of glucose metabolism prevents glycosylation of the glutamine transporter ASCT2 and promotes compensatory LAT1 upregulation in leukemia cells, *Oncotarget* 7(29) (2016) 46371-46383.

[35] C. Wong, T. Stylianopoulos, J. Cui, J. Martin, V.P. Chauhan, W. Jiang, Z. Popović, R.K. Jain, M.G. Bawendi, D. Fukumura, Multistage nanoparticle delivery system for deep penetration into tumor tissue, *Proceedings of the National Academy of Sciences* 108(6) (2011) 2426.

[36] S.H. Lee, J.S. Heo, H.J. Han, Effect of Hypoxia on 2-Deoxyglucose Uptake and Cell Cycle Regulatory Protein Expression of Mouse Embryonic Stem Cells: Involvement of  $Ca^{2+}$  /PKC, MAPKs and HIF-1 $\alpha$ , *Cellular Physiology and Biochemistry* 19(5-6) (2007) 269-282.